Inorganic Chemistry

pubs.acs.org/IC Forum Article

Energy Decomposition Analysis of Lewis Acid/Base Adducts and Frustrated Lewis Pairs: The Use of $E_{\rm Orb}/E_{\rm Steric}$ Ratios as a Reaction Parameter

Elon A. Ison* and Joshua L. Tubb



Cite This: https://doi.org/10.1021/acs.inorgchem.1c00911



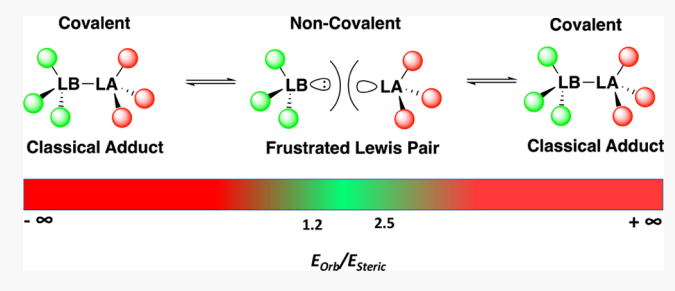
ACCESS I

III Metrics & More

Article Recommendations

S Supporting Information

ABSTRACT: The nature of bonding in classical adducts and frustrated Lewis pairs (FLPs) of oxorhenium and nitridorhenium complexes with $B(C_6F_5)_3$ was investigated computationally (B3PW91-D3). These studies have revealed that the primary noncovalent interaction (NCI) in the FLPs involves lone pair/ π interactions between the terminal M \equiv X bond and the aromatic C_6F_5 ring in $B(C_6F_5)_3$. Energy decomposition analyses on classical adducts and FLPs reveal that these species can be defined by the ratio (E_{Orb}/E_{Steric}) of covalent-to-noncovalent contributions to the total interaction energy, E_{Int} . This type of analysis reveals that



values for FLPs exist in a narrow range (1.2-2.5), with values for adducts significantly outside this range. The application of this method to other main-group combinations of Lewis acids and bases that have been shown to exhibit FLP reactivity yields similar results. These data suggest that similar NCIs are present in both transition-metal and main-group FLPs, especially where Lewis acids such as $B(C_6F_5)_3$ are utilized.

INTRODUCTION

In the past decade, frustrated Lewis pairs (FLPs) have emerged as an important area of research. 1-5 Many of these species are efficient for the activation of small molecules, and some of these species are catalytically active. 2,6 FLPs have been most prominently featured as species that can activate small molecules such as hydrogen, and many Lewis acid/base combinations have been shown to display this type of reactivity.7 As such, there have been numerous reports on the mechanism for H₂ splitting by FLPs. These mechanisms invariably involve the recognition that preorganization of the donor and acceptor sites via noncovalent interactions (NCIs) between the bulky substituents of the FLP is critical for the stability of these species. Some studies have attempted to shed light on the various factors influencing the formation and stability of FLP systems^{9,10} and to assess the importance of NCIs. The nature (structure and bonding) of chemical species in the preorganized donor/acceptor sites is still not well understand, however, because, unlike classical adducts, there is no covalent bond between the acid/base moieties. Further, there is a lack of systematic studies on the relative importance of the different types of NCIs (hydrogen-bonding, dipole/ dipole interactions, etc.) and the extent of these varying types of interactions in these systems.

Initial studies seemed to suggest that the occurrence of a covalent bond between a Lewis acid and base precluded the formation of a FLP. However, several Lewis acid/base adducts have now been shown to exhibit FLP reactivity, suggesting that

the absence of a covalent bond between the Lewis acid and base is not a requirement for reactivity. 11-17 It is clear that classical Lewis adducts and FLPs can exist in equilibrium, with a FLP occurring on a continuum along the reaction coordinate for Lewis acid—Lewis base bond formation, with bonding in an adduct primarily covalent and bonding in the adduct primarily noncovalent (Figure 1). However, there is no current method that would allow for the assessment of where a given Lewis acid/base pair combination is along this continuum.

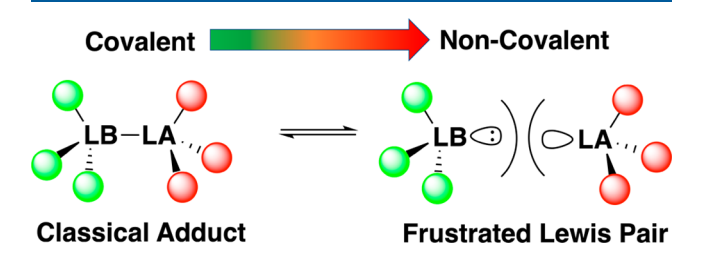


Figure 1. Equilibrium between classical adducts and FLPs.

Special Issue: Advances in Small-Molecule Activation

Received: March 24, 2021

A few recent examples exemplify the current understanding in the field. A model for Lewis acid/base interaction in a FLP was presented by Pápai and co-workers, who used density functional theory (DFT) calculations to suggest that the associated complex in a $tBu_3P/B(C_6F_5)_3$ FLP system was loosely maintained primarily by hydrogen bonding between H atoms at tBu_3P and F atoms at $B(C_6F_5)_3$, together with some additional stabilization from intermolecular dispersive interactions. In later studies, molecular dynamics simulations suggested that only a small fraction (\sim 2% at room temperature in toluene) of the $tBu_3P/B(C_6F_5)_3$ species were associated with each other. 19

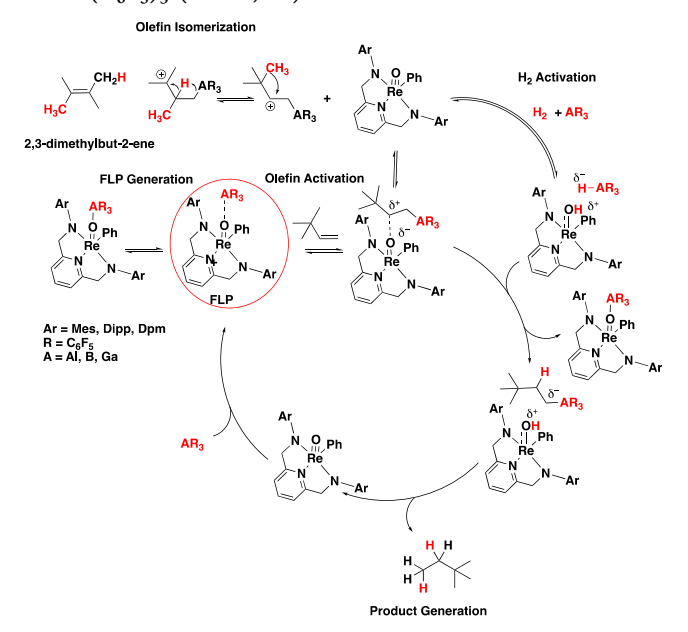
In 2009, Rhee and co-workers proposed an alternative model for NCIs in FLPs. Noting that the presumed stabilization from H–F hydrogen bonding was only \sim 2 kcal/mol per hydrogen bond when the P and B atoms were aligned at an idealized angle of 180° and that, in the optimized structure for this FLP, this angle is offset by 30°, it was suggested that hydrogen bonding could only account for a small percentage of the stabilization in FLPs. Instead, it was proposed that the stabilization is driven by a lone pair (from tBu₃P) to π orbital [from the C₆F₅ group in B(C₆F₅)₃] interaction because a significant binding energy of \sim 12 kcal/mol was calculated using the SCS-MP2 methods. This value is comparable to π/π interaction energies between small aromatic compounds. Further, it was proposed that the soft interaction causes an entropic stabilization in the FLP system in comparison to classic Lewis pairs.

Compared to main-group FLP chemistry, transition-metal FLPs are far less common. Transition-metal complexes and their reactions are well established, and the ease of synthesis and ligand modification allows for fine-tuning of the metal center both sterically and electronically. Transition-metal FLPs could also lead to the development of efficient catalytic systems that are complementary to main-group FLPs. The concept of transition-metal FLPs has been explored by the groups of Wass, Erker, Stephan, and Berke, and examples of transition-metal FLP complexes incorporating Ti, Zr, Zr, Hf, Ru, Tand Re. have been reported. In addition, recently traditional metal-only FLPs have been reported.

Recently, our laboratory has developed a program based on transition-metal oxo as the Lewis base component of FLPs. In 2013, we showed that oxorhenium complexes that incorporate diamidoamine (DAAm; N,N-bis(2-arylaminoethyl)methylamine, where ary C_6F_5 and Mes) and diamidopyridine (DAP) ligands form classical Lewis acid/base adducts with $B(C_6F_5)_3$. FLPs were generated from these adducts and resulted in species that were active in the activation of hydrogen and the catalytic hydrogenation of unactivated olefins.³¹ The mechanism for olefin activation with catalysts generated from O\Re(\text{Mes}DAP)(Ph) \text{Mes}DAP = \text{pyridine} 2,6-diylbis(methylene)]bis(mesitylamide)] and $B(C_6F_5)_3$ is summarized in Scheme 1 and involves the thermal generation of a FLP from the classical adduct $(C_6F_5)_3B\cdot O \equiv Re^{(Mes}DAP)$ -(Ph), which then activates H2 and the olefinic substrate. Despite these studies, the factors stabilizing the interaction between $O \equiv Re(^{Mes}DAP)(Ph)$ and $B(C_6F_5)_3$ have not been systematically investigated.

In this paper, we investigated the nature of the NCIs in FLPs generated from oxo- and nitridorhenium complexes and the Lewis acid $B(C_6F_5)_3$. To do this, we performed energy decomposition analysis (EDA) of the interaction energy between the Lewis basic transition-metal complex and Lewis

Scheme 1. Proposed Mechanism for the Hydrogenation of Olefins with the FLP Generated from $O \equiv Re^{(Mes}DAP)(Ph)$ and $A(C_6F_5)_3$ (A = B, Al)



acid. We also performed this analysis for several main-group FLPs that utilize $B(C_6F_5)_3$ as the Lewis acid component. These calculations reveal that FLPs can be easily identified and distinguished from classical Lewis adducts using this type of EDA. Most importantly, data suggest that NCIs in transition-metal FLPs are stabilized by similar interactions in main-group FLPs that feature perfluorinated ligands in the Lewis acid component.

■ RESULTS AND DISCUSSION

To understand the nature and extent of NCIs in FLPs generated from oxorhenium complexes and $B(C_6F_5)_3$, we investigated these species with computational methods. To do this, we investigated the equilibrium between the classical adduct and FLP (Scheme 2).

Scheme 2. Equilibrium between the Classical Adduct and FLP for $B(C_6F_5)_3/O \equiv Re(^{Mes}DAP)(Ph)$

The transition state (TS) for this equilibrium was located, and the classical adduct and FLP were identified as minima that were connected through vibrational analysis to this TS. We have previously shown that the oxorhenium complexes $O \equiv Re(^{Mes}DAP)(X)$ (X = H, 1; Me, 2, Ph, 3) readily form adducts with the Lewis acid $B(C_6F_5)_3$. From the X-ray crystal structures for these species, a typical B–O bond length of 1.54 Å and a Re–O–B bond angle of 173° were observed. Structures for these adducts were optimized by DFT

(B3PW91-D3), and relaxed potential energy surface scans were performed by varying the B–O bond lengths. These calculations resulted in new minima where the oxorhenium complex (Lewis base) and $B(C_6F_5)_3$ (Lewis acid) were weakly associated.³¹ Structures for the species $(C_6F_5)_3B\cdot O \equiv Re^{(Mes}DAP)(X)$ (X = H, 4; Me, 5; Ph, 6) are depicted in Figure 2.

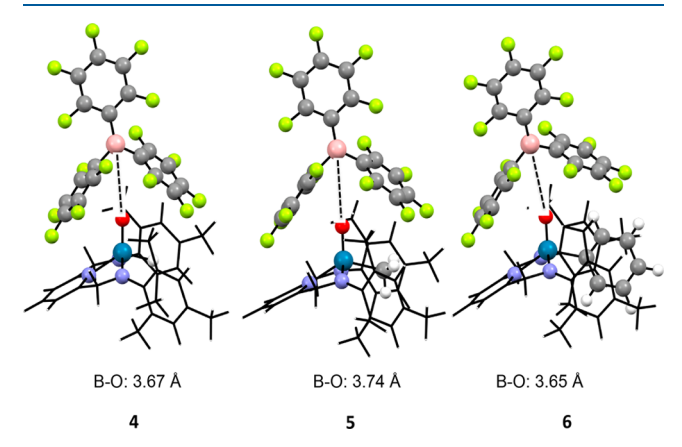


Figure 2. Optimized structures (B3PW91-D3) for $(C_6F_5)_3B\cdot O \equiv Re(^{Mes}DAP)(X)$ (X = H, 4; Me, 5; Ph, 6).

The most important characteristic of these structures is the long B–O contacts (3.67 Å, X = H; 3.74 Å, X = Me; 3.65 Å, X = Ph). In the optimized structure for these FLPs (typified by 6; Figure 3), the aryl–boron–aryl angle is condensed (114°)

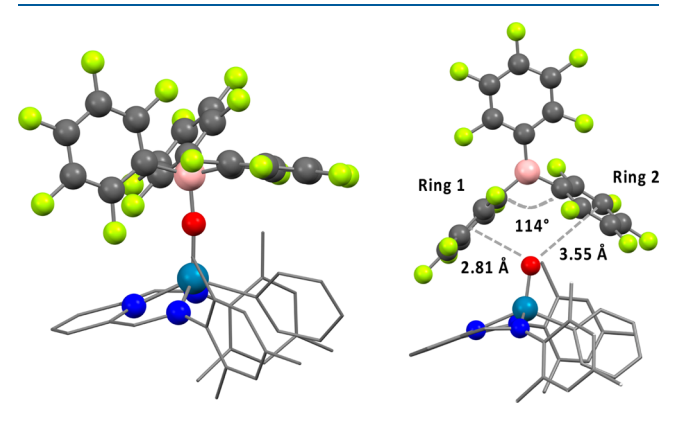


Figure 3. Optimized (B3PW91-D3) structures for the adduct and FLP generated from $B(C_6F_5)_3 \cdot O \equiv Re(^{Mes}DAP)(Ph)$.

between two of the C_6F_5 rings and seems to directly interact with the Re \equiv O bond. In contrast, the angle between other aryl–boron–aryl bonds that do not directly interact with the oxo ligand is approximately 123°. Close contacts between two of the C_6F_5 rings and the oxo ligand are observed (2.81 Å for one ring and 3.55 Å for the other). In addition, the empty p orbital on boron is orthogonal to the oxo ligand. These data suggest that there is a strong interaction between the lone pair on the oxo ligand and the C_6F_5 ring in $B(C_6F_5)_3$ structures.

To investigate this further, we performed a series of calculations where the F atoms in 6 were systematically replaced with H atoms. As shown in Figure 4, the distance between ring 1 (originally at a distance of 2.81 Å) increases as F atoms are replaced by H atoms. At the same time, the distance between ring 2 (originally at a distance of 3.55 Å) and

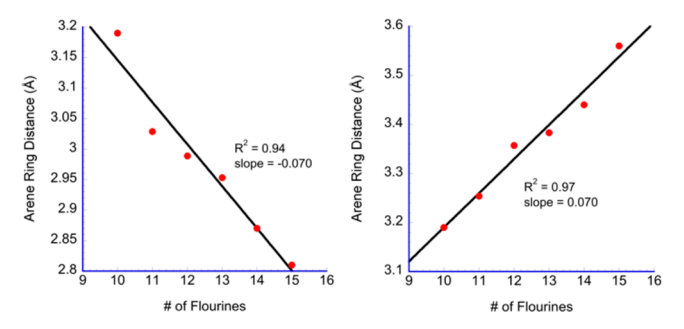


Figure 4. Plot showing the effect of fluorine substitution on the FLP $(C_6F_5)_3B/O\equiv Re(^{Mes}DAP)(Ph)$. The two plots show the distance of each ring in the $B(C_6F_5)_3$ fragment to the oxo ligand. The distance to ring 1 is in the left panel; the distance to ring 2 is in the right panel.

the oxo ligand decreases. This further reinforces the idea that the stabilizing interaction in these FLPs is likely due to an attractive interaction between the lone pair on the oxo ligand and the highly electron-deficient C_6F_5 rings in the Lewis acid $B(C_6F_5)_3$.

Unlike benzene, where the quadrupole moment is large and negative $(-29.0 \times 10^{-40} \text{ C m}^2)$, 32 the electronegativity of fluorine results in a quadrupole moment for hexafluorobenzene that is large and positive $(31.7 \times 10^{-40} \text{ C m}^2)^{32}$ (Figure 5). The electrostatic interaction energy in the FLP between $O \equiv \text{Re}(^{\text{Mes}}\text{DAP})(\text{Ph})$ and $B(C_6F_5)_3$ is therefore maximized, where the positive quadrupole moment of the C_6F_5 ring interacts with the negative quadrupole of the Re \equiv O bond (Figure 5).

To illustrate this further, a potential energy curve was generated by performing a relaxed potential energy surface scan and varying the distance of the Re \equiv O bond in O \equiv Re(MesDAP)(Ph) to hexafluorobenzene, which was used as a model for the C₆F₅ rings in the Lewis acid B(C₆F₅)₃. As shown in Figure 6, a minimum occurs at approximately 2.81 Å, similar to the distance observed for ring 1 in the optimized structure for 6. The data suggest that the polar nature of the Re \equiv O bond in these complexes is critical in stabilizing the FLP 6.

EDA. To gain a better understanding of the extent and nature of NCIs in FLPs, the EDA of Morokuma and Ziegler, as implemented in Gorelsky's AOMix~6.0 program, was utilized. ^{32–35} In this method, the electronic interaction energy, $E_{\rm Int}$, between two fragments is given by

$$E_{\rm Int} = E_{\rm Steric} + E_{\rm Orb}$$

where $E_{\text{Steric}} = \text{electrostatic energy} + \text{exchange repulsion energy}$

where E_{Orb} = orbital interaction energy

The E_{Steric} term describes the relative impact of NCIs, while the E_{Orb} term describes the covalent interactions. For the E_{Steric} term, the electrostatic energy is attractive, while the exchange repulsion energy is repulsive. This leads to situations where the E_{Steric} term can be either attractive or repulsive depending on the dominating interaction. The E_{Orb} term, on the other hand, is always attractive.

EDA was performed on several main-group molecules that have been shown to display FLP reactivity as well as the adduct generated from the oxorhenium complex 3 and the nitridorhenium complex ($^{\rm tBu}{\rm PNP}$)Re(N)(Me)·B(C₆F₅)₃ [PNP = bis[2-(di-tert-butylphosphanyl)ethyl]amide; Chart 1]. $^{\rm t1,13,14,17}$ The EDA results (Table 1) show that, for all

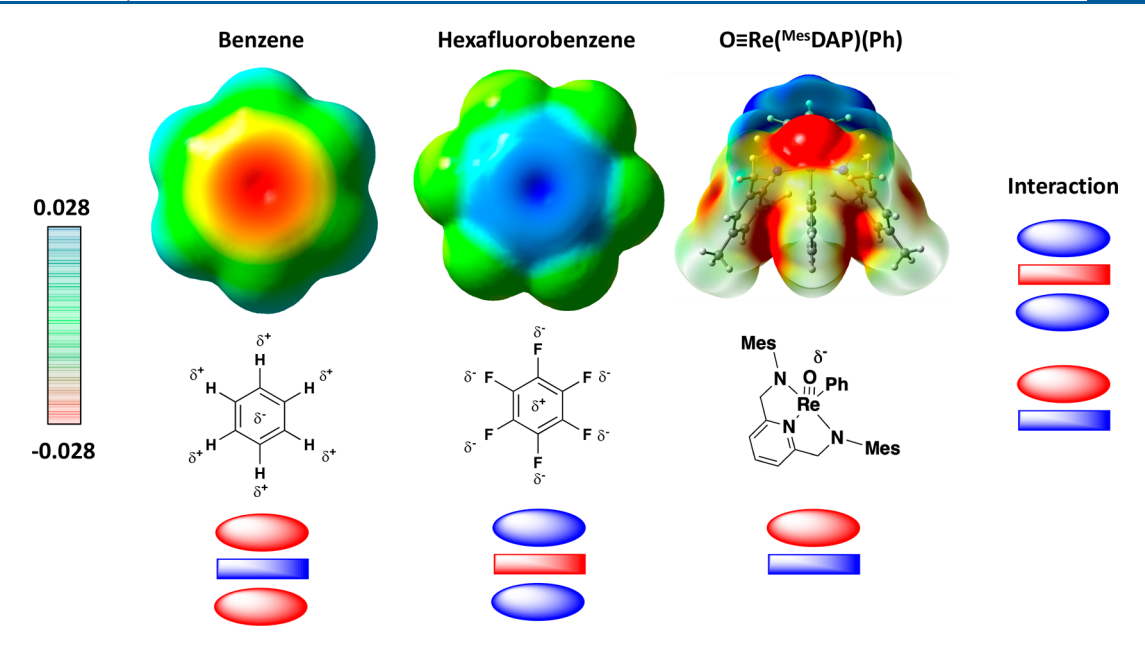


Figure 5. Electrostatic potential maps for benzene, hexafluorobenzene, and $O \equiv Re(^{Mes}DAP)(Ph)$. Cartoons depict the electron density above and below the plane.

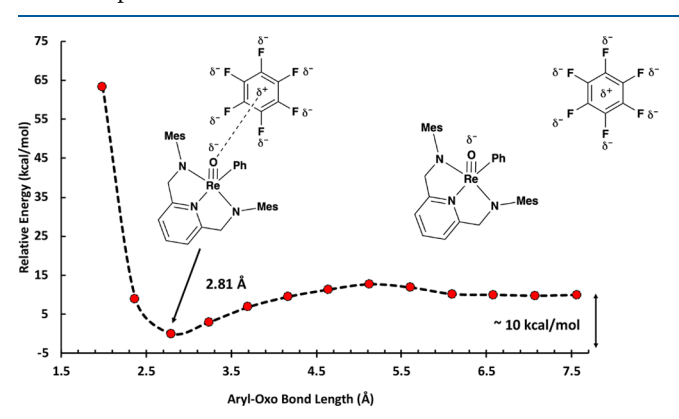


Figure 6. Potential energy curve (B3PW91-D3) for the interaction of $O \equiv Re^{(Mes}DAP)(Ph)$ with C_6F_6 .

adducts with $B(C_6F_5)_3$, the total interaction energy, E_{Intv} contains one stabilizing contribution, the orbital interaction energy, E_{Orb} , and one repulsive term, E_{Steric} (entries 1–6). This is consistent with the presence of a covalent bond in these adducts and steric repulsion as a result of bulky substituents on both the Lewis acid and base.

In contrast, the EDA results for FLPs generated from these adducts are depicted in Table 2 and show that the total interaction energy, $E_{\rm int}$ is composed of stabilizing contributions from both the orbital interaction energy and the $E_{\rm Steric}$ term. This is best illustrated by comparing the $E_{\rm Orb}/E_{\rm Steric}$ ratios for the adduct and FLP generated from 3 and B(C₆F₅)₃. For the adduct (Table 1, entry 5), the $E_{\rm Orb}/E_{\rm Steric}$ ratio is -2.6. In contrast, for the FLP, this ratio is 1.3 (Table 2, entry 9). This latter result reflects the stabilizing contributions from the $E_{\rm Steric}$ term and is consistent with the fact that the electrostatic energy is more significant than the exchange repulsion energy, as illustrated by the lone pair/ π interaction observed in 6. Lone pair/ π interactions are also evident in other rhenium species because an $E_{\rm Orb}/E_{\rm Steric}$ ratio of 1.8 was observed for the nitridorhenium FLP ($^{\rm IBu}$ PNP)Re(N)·B(C₆F₅)₃ (7).

Chart 1. Main-Group Molecules as Well as Oxorhenium and Nitridorhenium Complexes Used as Lewis Bases in FLPs

To examine this further, we performed similar analyses on FLPs and adducts of group 13 analogues of $B(C_6F_5)_3$, specifically $Al(C_6F_5)_3$ and $Ga(C_6F_5)_3$, with the nitridorhenium complex 7 as the Lewis base component. As shown in Table 1 (entries 7 and 8), the total interaction energies, $E_{\rm Int}$, for adducts of aluminum and gallium Lewis acids are dominated by the orbital interaction energy term, $E_{\rm Orb}$, while the $E_{\rm Steric}$ term is significantly smaller. This is consistent with the larger radii of these atoms, and as a consequence, the longer Re \equiv N—M bonds in these adducts, which results in reduced steric interactions between the *tert*-butyl substituents on the ligand and the C_6F_5 groups on $M(C_6F_5)_3$ (Figure 7).

EDA for the corresponding FLPs with 7 and Al(C_6F_5)₃ and Ga(C_6F_5)₃ is shown in Table 2. In contrast to adducts, the $E_{\rm Orb}$ and $E_{\rm Steric}$ terms are similar in sign and magnitude. The total

Table 1. EDA for Classical Lewis Adducts with $M(C_6F_5)_3$ (M = B, Al, Ga) and Several Main-Group Lewis Bases as Well as the Oxorhenium Complex 3 and Nitridorhenium Complex 7^a

entry	complex	$E_{\mathrm{Int}}^{}b}$	E_{Orb}^{b}	$E_{ m Steric}^{b}$	$E_{\mathrm{Orb}}/E_{\mathrm{Steric}}$
1	lutidine	-68.2	-105.4	37.2	-2.8
2	NHC ^c	-106.3	-125.9	19.6	-6.4
3	NMe_2Bn	-62.3	-82.8	20.5	-4.0
4	tBuBnNH	-80.2	-107.0	26.8	-4.0
5	3	-75.1	-121.8	46.7	-2.6
6	7	-97.2	-149.7	52.5	-2.8
7	7^d	-90.1	-81.1	-9.0	9.0
8	7^e	-78.2	-76.2	-2.0	37.5
9	8	-83.68	-119.5	35.8	-3.3

^aCalculations performed with the B3PW91-D3 functional and 6-311G basis set with $B(C_6F_5)_3$ as the Lewis acid. ^bEnergies are in kcal/mol. ^cNHC = 1,3-di-*tert*-butyl-1*H*-imidazol-3-ium-2-ide. ^dCalculations with $A(C_6F_5)_3$. ^eCalculations with $G(C_6F_5)_3$.

Table 2. EDA for FLPs with $M(C_6F_5)_3$ (M = B, Al, Ga) and Several Main-Group Lewis Bases as Well as the Oxorhenium Complex 3 and Nitridorhenium Complex 7^a

entry	complex	E_{Int}^{b}	$E_{\mathrm{Orb}}^{}b}$	$E_{ m Steric}^{b}$	$E_{\mathrm{Orb}}/E_{\mathrm{Steric}}$
1	lutidine	-16.3	-9.8	-6.5	1.5
2	NHC ^c	-16.9	-10.2	-6.7	1.5
3	NMe_2Bn	-14.7	-10.5	-4.2	2.5
4	quinoline	-15.2	-8.3	-6.9	1.2
5	tBuBnNH	-17.5	-11.9	-5.6	2.1
6	Ph_3P	-21.5	-11.8	-9.7	1.2
7	Mes_3P	-25.2	-13.9	-11.3	1.2
8	tBu_3P	-21.9	-13.8	-8.1	1.7
9	3	-32.7	-18.4	-14.	1.3
10	7	-31.3	-19.9	-11.4	1.8
11	7^d	-35.6	-20.8	-14.8	1.4
12	7^e	-35.6	-20.8	-14.8	1.4
13	8	-34.9	-22.8	-12.1	1.9

^aCalculations performed with the B3PW91-D3 functional and 6-311G basis set with $B(C_6F_5)_3$ as the Lewis acid. ^bEnergies are in kcal/mol. ^cNHC = 1,3-di-*tert*-butyl-1*H*-imidazol-3-ium-2-ide. ^dCalculations with $Al(C_6F_5)_3$. ^cCalculations with $Ga(C_6F_5)_3$.

interaction energy is composed two attractive terms ($E_{\rm Orb}$ and $E_{\rm Steric}$) and significantly, the ratio $E_{\rm Orb}/E_{\rm Steric}$ is 1.4. This is consistent with the absence of covalent bonds in the FLP structures, and, importantly, the data suggest that similar types of NCIs are present in the oxo complexes 3 and nitrido complexes 7.

In contrast, for classical Lewis adducts, the $E_{\rm Orb}/E_{\rm Steric}$ ratios were significantly outside this range (Table 1). These data indicate that while there is a continuum of values for the E_{Orb} / E_{Steric} ratios, the structures that can be regarded as FLPs fall within a very narrow range. Thus, this type of EDA can be used to quickly characterize whether a given combination of Lewis acid and Lewis base forms an FLP or an adduct. To illustrate this, we have also evaluated the rhenium hydride HRe(NO)- $(P(^{i}Pr_{3})_{2})Br(8)$, which with $B(C_{6}F_{5})_{3}$, was reported to display FLP reactivity in its reactions with CO₂. ²⁸ As shown in Table 1, the adduct of 8 and $B(C_6F_5)_3$ has an E_{Orb}/E_{Steric} ratio of -3.3, while the FLP generated from this combination has an $E_{\rm Orb}/E_{\rm Steric}$ ratio of 1.9 (Table 2). Inspection of the optimized structures (Figure 8) reveals the presence of a strong B-H bond (1.36 Å), while in the FLP, an NCI between the Re-H fragment and a perfluorinated aryl ring from B(C₆F₅)₃ is observed (3.15 Å).

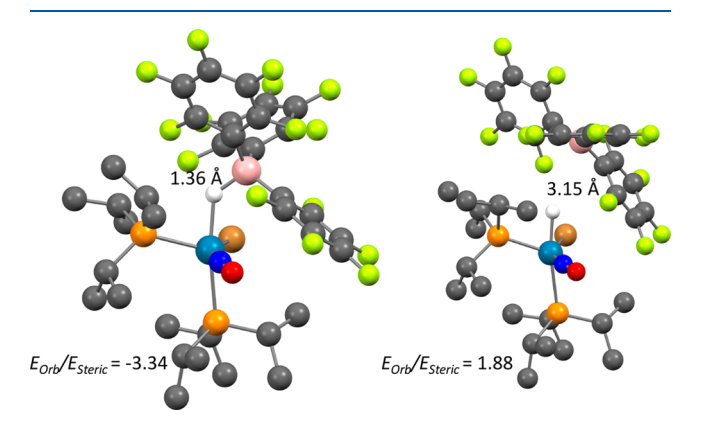


Figure 8. Optimized structures (B3PW91-D3) for adducts and FLPs for **8** and the Lewis acid $B(C_6F_5)_3$: (a) adduct; (b) FLP. Isopropyl substituents are shown as wireframes for clarity.

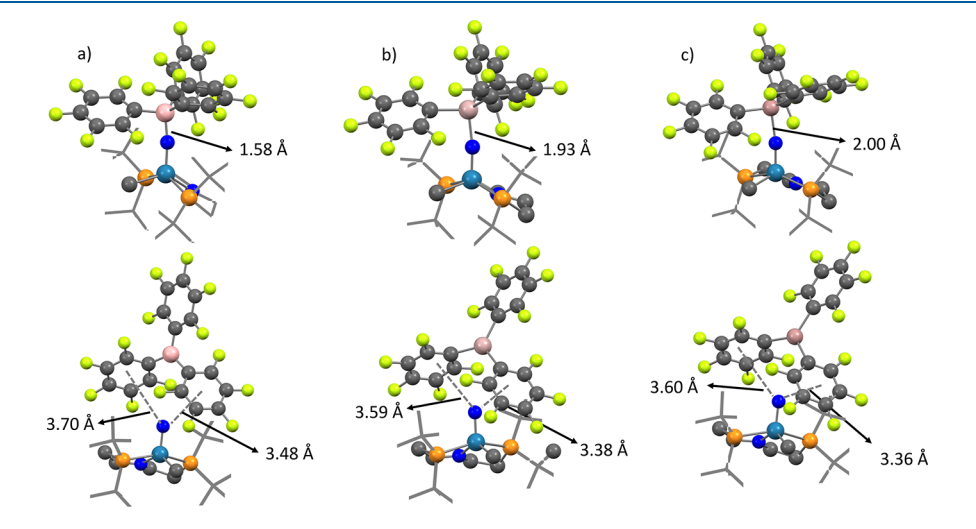


Figure 7. Optimized structures (B3PW91-D3) for the adducts and FLPs for 7 and the Lewis acids $M(C_6F_5)_3$: (a) M=B, adduct (top), FLP (bottom); (b) M=Ga, adduct (top), FLP (bottom); (c) M=Al, adduct (top), FLP (bottom). *tert*-Butyl substituents are shown as wireframes for clarity.

This type of analysis can also be correlated with reactivity, as we have recently shown with complexes [DAAmRe(CO)- $(NCCH_3)_2$ ⁺ [DAAm = N, N-bis(2-arylaminoethyl)methylamine; aryl = C₆F₅, Ph, Mes], which generate FLPs/ adducts with organosilanes and are catalytically active for the hydrosilylation of benzaldehyde.³³ The most active catalyst (aryl = C_6F_5) has a E_{Orb}/E_{Steric} ratio 1.1, while catalysts with phenyl and mesityl substituents have less FLP character with ratios of -2.4 and 7.9, respectively, which is consistent with their diminished reactivity. To expand on this, the $E_{\rm Orb}/E_{\rm Steric}$ ratios for Lewis acid/base combinations consisting of the group 13 Lewis acids $M(C_6F_5)_3$ (M = B, Ga, Al) and Me₂PhSiH were obtained. Again, the TS for the conversion of covalently bound species to noncovalently bound species was obtained, and EDA of the minima associated with the TS was performed. Minima associated with this transformation included species that contained covalently bound Si-H/M bonds with M-H bond lengths of 1.52, 1.75, and 1.80 Å for the B, Ga, and Al species, respectively. These species are best characterized as adducts and display $E_{\rm Orb}/E_{\rm Steric}$ ratios of -2.3, -6.6, and -51.3 (entries 4-6) for the B, Ga, and Al species (Table 3). These adducts are in equilibrium with species that

Table 3. EDA for Lewis Acid/Base Combinations Consisting of the Group 13 Lewis Acids $M(C_6F_5)_3$ (M = B, Ga, Al) and Me_2PhSiH^a

entry	$M(C_6F_5)_3$	M–H covalent bond	$E_{ m Int}$	E_{Orb}	$E_{ m Steric}$	$E_{ m Orb}/$ $E_{ m Steric}$
1	M = Al	no	-40.2	-40.5	0.33	-123
2	M = B	no	-16.4	-8.8	-7.6	1.2
3	M = Ga	no	-34.2	-36.9	2.8	-13.4
4	M = Al	yes	-35.2	-35.9	0.7	-51.3
5	M = B	yes	-30.1	-52.5	22.4	-2.3
6	M = Ga	yes	-32.3	-38.1	5.8	-6.6

 a Calculations were performed with the B3PW91-D3 functional and 6-311G basis set.

do not contain a Si–H/M bond, as shown in Figure 9. The EDA results (Table 3) for the B, Ga, and Al species are 1.2, -13.4, and -123, respectively. Only the B(C_6F_5)₃/silane combinations are known to catalyze the hydrosilylation of ketones.³⁴

The optimized structures for noncovalently bound M- $(C_6F_5)_3$ (M = B, Ga, Al) species are depicted in Figure 9. In addition, natural bond orbital (NBO)³⁵ analysis reveals donor/acceptor interactions between the aromatic π orbitals from the Me₂PhSiH donor to the empty p orbital in M(C_6F_5)₃ (Figure 10). The second-order perturbation stabilization energy,

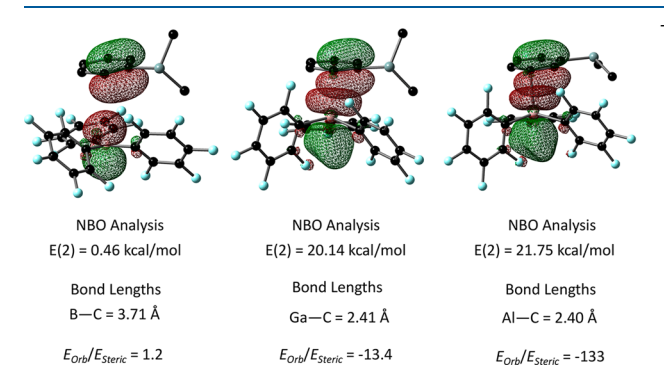


Figure 10. NBOs for $M(C_6F_5)_3$ (M = B, Ga, Al) interacting with Me_2PhSiH . Plots depict donor/acceptor interactions from the Me_2PhSiH donor [NBO = 159 (a), 173 (b), and 160 (c)] to the empty orbital (lone valency) on M in $M(C_6F_5)_3$ [NBO = 174 (a), 187 (b), and 181 (c)]. Plots are depicted with an isovalue of 0.045. The second-order perturbation stabilization energy, $\Delta E(2)$, was obtained from the *NBO 7.0* program, ³⁵ as implemented in *Gaussian 09*.

 $\Delta E(2)$, is 0.46, 20.14, and 21.75 kcal/mol respectively for the B, Ga, and Al species; i.e., the stabilization from the aromatic p electrons to the empty p orbital is strongest for Ga and Al. Consistent with this, the M–C bond lengths of 3.71, 2.41, and 2.40 Å for B, Ga, and Al, respectively, were observed for these species. The bond lengths for Ga and Al are larger

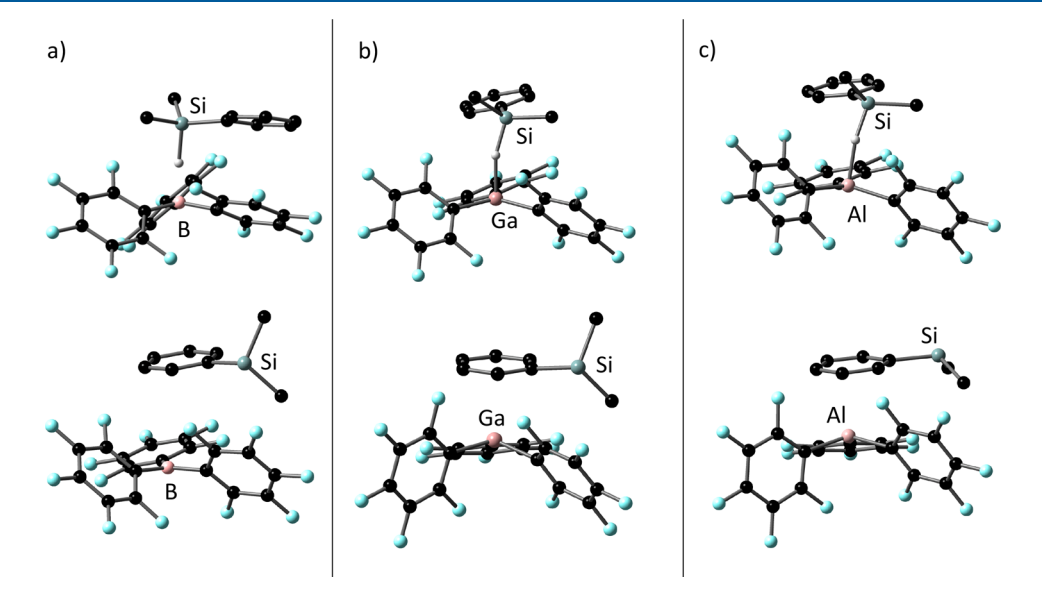


Figure 9. Optimized structures (B3PW91-D3) for Lewis acid/base combinations consisting of the group 13 Lewis acids $M(C_6F_5)_3$ (M = B, Ga, Al) and Me_2PhSiH . For molecules in the top row, there is a covalent bond between the Lewis acid and Si-H. In the bottom row, no Si-H/M bond is evident.

than the sum of the covalent radii for Ga, Al, and C atoms and longer than the average Ga–C (1.993 \pm 0.069 Å) and Al–C (2.00 \pm 0.038 Å) bond lengths. Thus, the presence of covalent bonds in these species is somewhat ambiguous. However, EDA suggests that the interaction energy, $E_{\rm Int}$, is dominated by the orbital interaction energy, $E_{\rm Orb}$, which represents covalent bonding, while the noncovalent $E_{\rm Steric}$ term is quite small. Thus, the Ga and Al analogues are stabilized by weak covalent interactions between the Me₂PhSiH aromatic groups and the empty p orbitals on Ga and Al. The $E_{\rm Orb}/E_{\rm Steric}$ ratios of -13.4 and -133 obtained for these species justifiably place them outside the desired range for reactive FLPs.

The B analogue, on the other hand, appears to be stabilized by aromatic π/π interactions between the one aryl ring on Me₂PhSiH and one perfluorinated ring in $B(C_6F_5)_3$. There is unambiguously no B-C bond within this species, and NBO analysis reveals a minimal overlap of the aromatic π orbitals in Me₂PhSiH and the empty p orbital on B. Most importantly from EDA, the two components of the interaction energy, E_{Orb} and E_{Steric} , are almost equal and result in an $E_{\text{Orb}}/E_{\text{Steric}}$ ratio of 1.2. Thus, of the three minima generated from the adducts Me₂PhSiH and M(C₆F₅)₃, only the B analogue can be regarded as an FLP. Indeed, it is only this species, when combined with organosilanes, that has been shown to exhibit FLP reactivity. These results suggest that, for a variety of FLPs, the E_{Orb}/E_{Steric} ratio occurs within a narrow range of values, which reflects the fact than in these species the contribution from NCIs is significant and the contribution of covalent bonding to the overall interaction energy is diminished.

Inspection of the structures for many main-group FLPs reveals that they are stabilized by a variety of NCIs. As shown in Figure 11, lone pair/ π interactions are observed in FLPs

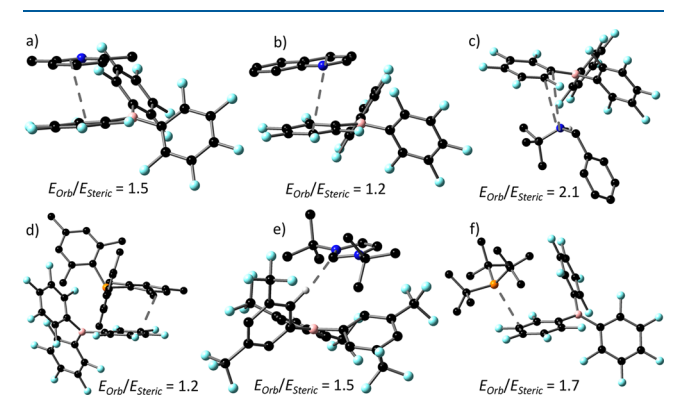


Figure 11. NCIs in FLPs generated from $B(C_6F_5)_3$ and (a) lutidene, (b) quinoline, (c) tBuBnNH, (d) Mes₃P, (e) NHC = 1,3-di-tert-butyl-1H-imidazol-3-ium-2-ide with B[3,5-(CF₃)(C₆H₃)], and (f) tBu₃P. Close contacts (Å) lutidine (aromatic)—aromatic $(C_6F_5)_3B$ (3.45); quinoline (aromatic)—aromatic $(C_6F_5)_3B$ (3.60); tBuBnNH (lp)—aromatic $(C_6F_5)_3B$ (3.17 and 3.40); Mes₃P (aromatic)—aromatic $(C_6F_5)_3B$ (3.70); NHC (lp)—B[3,5-(CF₃)(C₆H₃)] (H) (2.27); tBu₃P (lp)—aromatic $(C_6F_5)_3B$ (3.46 and 3.49).

generated from tBuBnNH, tBu₃P, and B(C_6F_5)₃. For species generated from quinoline and lutidine, aromatic donors/ acceptors are observed. Hydrogen-bonding interactions are observed for the FLP generated from the NHC Lewis base 1,3-di-*tert*-butyl-1*H*-imidazol-3-ium-2-ide and the Lewis acid B(3,5-(CF_3)-(C_6H_3))₃. Importantly, the E_{Orb}/E_{Steric} ratios for these FLPs fall within a very narrow range of 1.2–2.5 (Table 1), while the ratios for adducts are significantly outside this

range (Table 2), regardless of the nature of the NCI. Thus, partitioning of the interaction energy into the two terms $E_{\rm Orb}$ and $E_{\rm Steric}$ allows for the rapid assessment of the relative magnitudes of covalent versus noncovalent bonding interactions because all NCIs are absorbed into the $E_{\rm Steric}$ term.

CONCLUSIONS

Lone pair/ π interactions account for the stability of FLPs generated from oxo- and nitridorhenium complexes and the Lewis acids $M(C_6F_5)_3$ (M = B, Al, Ga). The stabilizing interaction in these FLPs is likely due to an attractive interaction between the lone pair on the oxo/nitrido ligand and the highly electron-deficient C_6F_5 rings in the Lewis acid $M(C_6F_5)_3$. EDA of the interaction energy between the Lewis basic transition-metal complex and the Lewis acid reveals that FLPs can be easily identified and distinguished from classical Lewis adducts by examining the ratio of the orbital interaction energy, E_{Orb} , to the electrostatic and exchange repulsion energy, $E_{\rm Steric}$. This analysis suggests that FLPs display $E_{\rm Orb}/$ E_{Steric} ratios in the narrow range of 1.2–2.5 and species that are best described as adducts exhibit $E_{\text{Orb}}/E_{\text{Steric}}$ ratios significantly outside this range. We have shown in the case of species derived from the Lewis acids $M(C_6F_5)_3$ (M = B, Ga, Al) and Me₂PhSiH that these ratios can be correlated with reactivity, in that only the B derivative displays an FLP in the desired range and is the only species in this family that is catalytically active for the hydrosilylation of ketones. We anticipate that this type of analysis may be used for other Lewis acid/base combinations to assess the correlation of the $E_{\rm Orb}/E_{\rm Steric}$ parameter with reactivity.

The analysis emphasizes the relative amount of covalent/ NCIs rather than the absolute strength of any one contribution to bonding. These calculations do not require a tremendous amount of computational resources and will be useful for practitioners in this field. Most importantly, data suggest that similar ratios are also evident in FLPs and adducts composed of main-group Lewis bases and the traditional Lewis acid $B(C_6F_5)_3$. Further, data suggest that NCIs in transition-metal and main-group FLPs that incorporate Lewis acids with perfluorinated ligands are similar in nature. Given the extensive utilization of $B(C_6F_5)_3$ and their derivatives in FLP chemistry, this type of simple analysis is potentially useful for the design of new catalytic systems.

EXPERIMENTAL SECTION

Computational Methods. Theoretical calculations have been carried out using the *Gaussian* 09^{37} implementation of B3PW91^{38,39} density functional theory with the D3 version of Grimme's empirical dispersion correction. ⁴⁰ All geometry optimizations were carried out in the gas phase using tight convergence criteria ("opt = tight") and pruned ultrafine grids ("Int = ultrafine"). The basis set for Re was the small-core (311111, 22111, 411) \rightarrow [6s5p3d] Stuttgart–Dresden basis set and relativistic effective core potential (RECP) combination (SDD) with an additional f polarization function. ^{41–54} The 6-31G(d,p) basis set was used for all other atoms. ⁵⁵

From the optimized structures of the adducts, relaxed potential energy surface scans were performed by increasing the bond distance between the Lewis acid (LA) and Lewis base (LB) until there was no longer a bond between the fragments. The maximum from this scan was then used to generate a guess for the TS for the equilibrium reaction:

$$LA - LB \stackrel{TS}{\rightleftharpoons} LA - -LB$$

The TS structure was then fully optimized, and analytical frequency calculations were performed to ensure a first-order saddle point. The minima associated with each TS were determined by animation of the imaginary frequency. In addition, analytical frequency calculations were used to ensure a zeroth-order saddle point (a local minimum). NBO analysis was performed with NBO 7.0, 35 as implemented in the Gaussian 09 program. Mulliken population analyses and EDA were performed using $AOMix~6.90.^{56,57}$ Energetics and EDA were calculated on the gas-phase-optimized structures, as described above with the $6.311G(d,p)^{58}$ basis set for nontransition metals and the SDD basis set with an added f polarization function on Re.

ASSOCIATED CONTENT

Supporting Information

The Supporting Information is available free of charge at https://pubs.acs.org/doi/10.1021/acs.inorgchem.1c00911.

Optimized geometries available in a single .xyz file (XYZ)

AUTHOR INFORMATION

Corresponding Author

Elon A. Ison — Department of Chemistry, North Carolina State University (NCSU), Raleigh, North Carolina 27695-8204, United States; orcid.org/0000-0002-2902-2671; Email: eaison@ncsu.edu

Author

Joshua L. Tubb – Department of Chemistry, North Carolina State University (NCSU), Raleigh, North Carolina 27695-8204, United States

Complete contact information is available at: https://pubs.acs.org/10.1021/acs.inorgchem.1c00911

Author Contributions

The manuscript was written through contributions of all authors. All authors have given approval to the final version of the manuscript.

Funding

This work was supported by NCSU and the National Science Foundation via Grant CHE-1664973.

Notes

The authors declare no competing financial interest.

ACKNOWLEDGMENTS

We acknowledge the NCSU Office of Information Technology High Performance Computing for computational support.

REFERENCES

- (1) Stephan, D. W.; Erker, G., Frustrated Lewis Pair Mediated Hydrogenations. *Frustrated Lewis Pairs I*; Springer, 2013; pp 85–110.
- (2) Stephan, D. W. Frustrated Lewis Pairs: from Concept to Catalysis. Acc. Chem. Res. 2015, 48, 306–316.
- (3) Stephan, D. W. Frustrated Lewis Pairs. J. Am. Chem. Soc. 2015, 137, 10018-10032.
- (4) Stephan, D. W.; Erker, G. Frustrated Lewis pair chemistry: development and perspectives. *Angew. Chem., Int. Ed.* **2015**, 54, 6400–6441.
- (5) Stephan, D. W. The Broadening Reach of Frustrated Lewis Pair Chemistry. *Science* **2016**, 354, aaf7229.
- (6) Paradies, J. From Structure to Novel Reactivity in Frustrated Lewis Pairs. Coord. Chem. Rev. 2019, 380, 170-183.
- (7) Grimme, S.; Kruse, H.; Goerigk, L.; Erker, G. The Mechanism of Dihydrogen Activation by Frustrated Lewis Pairs Revisited. *Angew. Chem., Int. Ed.* **2010**, 49, 1402–1405.

- (8) Daru, J.; Bakó, I.; Stirling, A.; Pápai, I. Mechanism of Heterolytic Hydrogen Splitting by Frustrated Lewis Pairs: Comparison of Static and Dynamic Models. ACS Catal. 2019, 9, 6049–6057.
- (9) Skara, G.; Pinter, B.; Top, J.; Geerlings, P.; De Proft, F.; De Vleeschouwer, F. Conceptual Quantum Chemical Analysis of Bonding and Noncovalent Interactions in the Formation of Frustrated Lewis Pairs. Chem. Eur. J. 2015, 21, 5510—5519.
- (10) Bannwarth, C.; Hansen, A.; Grimme, S. The Association of Two "Frustrated" Lewis Pairs by State-of-the-Art Quantum Chemical Methods. *Isr. J. Chem.* **2015**, *55*, 235–242.
- (11) Geier, S. J.; Stephan, D. W. Lutidine/B(C_6F_5)₃: At the Boundary of Classical and Frustrated Lewis Pair Reactivity. *J. Am. Chem. Soc.* **2009**, *131*, 3476–3477.
- (12) Fontaine, F.-G.; Stephan, D. W. On the Concept of Frustrated Lewis Pairs. *Philos. Trans. R. Soc., A* **2017**, *375*, 20170004.
- (13) Geier, S. J.; Gille, A. L.; Gilbert, T. M.; Stephan, D. W. From Classical Adducts to Frustrated Lewis Pairs: Steric Effects in the Interactions of Pyridines and $B(C_6F_5)_3$. *Inorg. Chem.* **2009**, 48, 10466–10474.
- (14) Schwendemann, S.; Oishi, S.; Saito, S.; Fröhlich, R.; Kehr, G.; Erker, G. Reaction of an "Invisible" Frustrated N/B Lewis Pair with Dihydrogen. *Chem. Asian J.* **2013**, *8*, 212–217.
- (15) Spies, P.; Fröhlich, R.; Kehr, G.; Erker, G.; Grimme, S. Structural Importance of Secondary Interactions in Molecules: Origin of Unconventional Conformations of Phosphine—Borane Adducts. *Chem. Eur. J.* **2008**, *14*, 333–343.
- (16) Voss, T.; Mahdi, T.; Otten, E.; Fröhlich, R.; Kehr, G.; Stephan, D. W.; Erker, G. Frustrated Lewis Pair Behavior of Intermolecular Amine/ $B(C_6F_5)_3$ Pairs. Organometallics **2012**, 31, 2367–2378.
- (17) Erős, G.; Nagy, K.; Mehdi, H.; Pápai, I.; Nagy, P.; Király, P.; Tárkányi, G.; Soós, T. Catalytic Hydrogenation with Frustrated Lewis Pairs: Selectivity Achieved by Size-Exclusion Design of Lewis Acids. *Chem. Eur. J.* **2012**, *18*, 574–585.
- (18) Stirling, A.; Hamza, A.; Rokob, T. A.; Pápai, I. Concerted attack of frustrated Lewis acid—base pairs on olefinic double bonds: a theoretical study. *Chem. Commun.* **2008**, 27, 3148—3150.
- (19) Bakó, I.; Stirling, A.; Bálint, S.; Pápai, I. Association of Frustrated Phosphine—Borane Pairs in Toluene: Molecular Dynamics Simulations. *Dalton Trans.* **2012**, *41*, 9023—9025.
- (20) Takatani, T.; Sherrill, C. D. Performance of Spin-Component-Scaled Møller–Plesset theory (SCS-MP2) for Potential Energy Curves of Noncovalent Interactions. *Phys. Chem. Chem. Phys.* **2007**, *9*, 6106–6114.
- (21) Martinez, C. R.; Iverson, B. L. Rethinking the Term "Pi-Stacking. Chem. Sci. 2012, 3, 2191–2201.
- (22) Flynn, S. R.; Wass, D. F. Transition Metal Frustrated Lewis Pairs. ACS Catal. 2013, 3, 2574–2581.
- (23) Normand, A. T.; Richard, P.; Balan, C. d.; Daniliuc, C. G.; Kehr, G.; Erker, G.; Le Gendre, P. Synthetic Endeavors Toward Titanium Based Frustrated Lewis Pairs With Controlled Electronic and Steric Properties. *Organometallics* **2015**, *34*, 2000–2011.
- (24) Chapman, A. M.; Haddow, M. F.; Wass, D. F. Frustrated Lewis Pairs Beyond the Main Group: Cationic Zirconocene–Phosphinoaryloxide Complexes and Their Application in Catalytic Dehydrogenation of Amine Boranes. *J. Am. Chem. Soc.* **2011**, *133*, 8826–8829.
- (25) Xu, X.; Kehr, G.; Daniliuc, C. G.; Erker, G. Formation of Unsaturated Vicinal Zr⁺/P Frustrated Lewis Pairs by the Unique 1, 1-Carbozirconation Reactions. *J. Am. Chem. Soc.* **2014**, *136*, 12431–12443
- (26) Chapman, A. M.; Haddow, M. F.; Wass, D. F. Cationic Group 4 Metallocene—(o-Phosphanylaryl) oxido Complexes: Synthetic Routes to Transition-Metal Frustrated Lewis Pairs. *Eur. J. Inorg. Chem.* **2012**, 2012, 1546—1554.
- (27) Sgro, M. J.; Stephan, D. W. Frustrated Lewis Pair Inspired Carbon Dioxide Reduction by a Ruthenium Tris(aminophosphine) Complex. *Angew. Chem., Int. Ed.* **2012**, *51*, 11343–11345.
- (28) Jiang, Y.; Blacque, O.; Fox, T.; Berke, H. Catalytic CO_2 Activation Assisted by Rhenium Hydride/B(C_6F_5)₃ Frustrated

- Lewis Pairs—Metal Hydrides Functioning as FLP Bases. J. Am. Chem. Soc. 2013, 135, 7751—7760.
- (29) Campos, J. Dihydrogen and Acetylene Activation by a Gold (I)/Platinum (0) Transition Metal Only Frustrated Lewis Pair. *J. Am. Chem. Soc.* **2017**, *139*, 2944–2947.
- (30) Smeltz, J. L.; Lilly, C. P.; Boyle, P. D.; Ison, E. A. The Electronic Nature of Terminal Oxo Ligands in Transition-Metal Complexes: Ambiphilic Reactivity of Oxorhenium Species. *J. Am. Chem. Soc.* **2013**, *135*, 9433–9441.
- (31) Lambic, N. S.; Sommer, R. D.; Ison, E. A. Transition-Metal Oxos as the Lewis Basic Component of Frustrated Lewis Pairs. *J. Am. Chem. Soc.* **2016**, *138*, 4832–4842.
- (32) Mallick, S.; Cao, L.; Chen, X.; Zhou, J.; Qin, Y.; Wang, G. Y.; Wu, Y. Y.; Meng, M.; Zhu, G. Y.; Tan, Y. N.; Cheng, T.; Liu, C. Y. Mediation of Electron Transfer by Quadrupolar Interactions: The Constitutional, Electronic, and Energetic Complementarities in Supramolecular Chemistry. *iScience* 2019, 22, 269–287.
- (33) Brown, C. A.; Abrahamse, M.; Ison, E. A. Re–Silane complexes as frustrated lewis pairs for catalytic hydrosilylation. *Dalton Trans.* **2020**, *49*, 11403–11411.
- (34) Parks, D. J.; Piers, W. E. Tris(pentafluorophenyl) Boron-Catalyzed Hydrosilation of Aromatic Aldehydes, Ketones, and Esters. J. Am. Chem. Soc. 1996, 118, 9440–9441.
- (35) Glendening, E. D.; Badenhoop, J. K.; Reed, A. E.; Carpenter, J. E.; Bohmann, J. A.; Morales, C. M.; Karafiloglou, P.; Landis, C. R.; Weinhold, F. *NBO 7.0*; Theoretical Chemistry Institute, University of Wisconsin: Madison, WI, 2018.
- (36) Groom, C. R.; Bruno, I. J.; Lightfoot, M. P.; Ward, S. C. The Cambridge Structural Database. *Acta Crystallogr., Sect. B: Struct. Sci., Cryst. Eng. Mater.* **2016**, 72, 171–179.
- (37) Frisch, M. J.; Trucks, G. W.; Schlegel, H. B.; Scuseria, G. E.; Robb, M. A.; Cheeseman, J. R.; Scalmani, G.; Barone, V.; Petersson, G. A.; Nakatsuji, H.; Li, X.; Caricato, M.; Marenich, A.; Bloino, J.; Janesko, B. G.; Gomperts, R.; Mennucci, B.; Hratchian, H. P.; Ortiz, J. V.; Izmaylov, A. F.; Sonnenberg, J. L.; Williams-Young, D.; Ding, F.; Lipparini, F.; Egidi, F.; Goings, J.; Peng, B.; Petrone, A.; Henderson, T.; Ranasinghe, D.; Zakrzewski, V. G.; Gao, J.; Rega, N.; Zheng, G.; Liang, W.; Hada, M.; Ehara, M.; Toyota, K.; Fukuda, R.; Hasegawa, J.; Ishida, M.; Nakajima, T.; Honda, Y.; Kitao, O.; Nakai, H.; Vreven, T.; Throssell, K.; Montgomery, J. A., Jr.; Peralta, J. E.; Ogliaro, F.; Bearpark, M.; Heyd, J. J.; Brothers, E.; Kudin, K. N.; Staroverov, V. N.; Keith, T.; Kobayashi, R.; Normand, J.; Raghavachari, K.; Rendell, A.; Burant, J. C.; Iyengar, S. S.; Tomasi, J.; Cossi, M.; Millam, J. M.; Klene, M.; Adamo, C.; Cammi, R.; Ochterski, J. W.; Martin, R. L.; Morokuma, K.; Farkas, O.; Foresman, J. B.; Fox, D. J. Gaussian 09, revision D.01; Gaussian, Inc.: Wallingford, CT, 2016.
- (38) Becke, A. D. Density-Functional Exchange-Energy Approximation with Correct Asymptotic Behavior. *Phys. Rev. A: At., Mol., Opt. Phys.* **1988**, *38*, 3098.
- (39) Becke, A. D. Density-Functional Thermochemistry. III. The Role of Exact Exchange. J. Chem. Phys. 1993, 98 (7), 5648-5652.
- (40) Grimme, S.; Antony, J.; Ehrlich, S.; Krieg, H. A Consistent and Accurate Ab Initio Parametrization of Density Functional Dispersion Correction (DFT-D) for the 94 elements H-Pu. *J. Chem. Phys.* **2010**, 132, 154104
- (41) Cao, X.; Dolg, M. Valence Basis Sets for Relativistic Energy-Consistent Small-Core Lanthanide Pseudopotentials. *J. Chem. Phys.* **2001**, *115*, 7348–7355.
- (42) Cao, X.; Dolg, M. Segmented Contraction Scheme for Small-Core Lanthanide Pseudopotential Basis Sets. *J. Mol. Struct.:* THEOCHEM **2002**, 581, 139–147.
- (43) Leininger, T.; Nicklass, A.; Stoll, H.; Dolg, M.; Schwerdtfeger, P. The Accuracy of the Pseudopotential Approximation. II. A Comparison of Various Core sizes for Indium Pseudopotentials in Calculations for Spectroscopic Constants of InH, InF, and InCl. J. Chem. Phys. 1996, 105, 1052–1059.
- (44) Nicklass, A.; Dolg, M.; Stoll, H.; Preuss, H. Ab Initio Energy-Adjusted Pseudopotentials for the Noble Gases Ne through Xe:

I

- Calculation of Atomic Dipole and Quadrupole Polarizabilities. *J. Chem. Phys.* **1995**, 102, 8942–8952.
- (45) Küchle, W.; Dolg, M.; Stoll, H.; Preuss, H. Energy-Adjusted Pseudopotentials for the Actinides. Parameter Sets and Test Calculations for Thorium and Thorium Monoxide. *J. Chem. Phys.* **1994**, *100*, 7535–7542.
- (46) Dolg, M.; Stoll, H.; Preuss, H.; Pitzer, R. M. Relativistic and Correlation Effects for Element 105 (Hahnium, Ha): a Comparative Study of M and MO (M = Nb, Ta, Ha) Using Energy-Adjusted Ab Initio Pseudopotentials. *J. Phys. Chem.* **1993**, 97, 5852–5859.
- (47) Häussermann, U.; Dolg, M.; Stoll, H.; Preuss, H.; Schwerdtfeger, P.; Pitzer, R. Accuracy of Energy-Adjusted Quasirelativistic Ab Initio Pseudopotentials: All-Electron and Pseudopotential Benchmark Calculations for Hg, HgH and Their Cations. *Mol. Phys.* 1993, 78, 1211–1224.
- (48) Fuentealba, P.; Von Szentpaly, L.; Preuss, H.; Stoll, H. Pseudopotential Calculations for Alkaline-Earth Atoms. *J. Phys. B: At. Mol. Phys.* **1985**, *18*, 1287.
- (49) Stoll, H.; Fuentealba, P.; Schwerdtfeger, P.; Flad, J. v.; Szentpály, L. v.; Preuss, H. Cu and Ag as One-Valence-Electron Atoms: CI Results and Quadrupole Corrections for Cu₂, Ag₂, CuH, and AgH. *J. Chem. Phys.* **1984**, *81*, 2732–2736.
- (50) Fuentealba, P.; Stoll, H.; Von Szentpaly, L.; Schwerdtfeger, P.; Preuss, H. On the Reliability of Semi-Empirical Pseudopotentials: Simulation of Hartree-Fock and Dirac-Fock Results. *J. Phys. B: At. Mol. Phys.* **1983**, *16*, L323.
- (51) von Szentpaly, L.; Fuentealba, P.; Preuss, H.; Stoll, H. Pseudopotential Calculations on Rb⁺², Cs⁺², RbH⁺, CsH⁺ and the Mixed Alkali Dimer Ions. *Chem. Phys. Lett.* **1982**, *93*, 555–559.
- (52) Fuentealba, P.; Preuss, H.; Stoll, H.; Von Szentpaly, L. A Proper Account of Core-Polarization with Pseudopotentials: Single Valence-Electron Alkali Compounds. *Chem. Phys. Lett.* **1982**, *89*, 418–422.
- (53) Dunning, T. H.; Hay, P. J. Methods of Electronic Structure Theory. *Modern Theoretical Chemistry* **1977**, 3, 1–28.
- (54) Ehlers, A.; Böhme, M.; Dapprich, S.; Gobbi, A.; Höllwarth, A.; Jonas, V.; Köhler, K.; Stegmann, R.; Veldkamp, A.; Frenking, G. A Set of f-Polarization Functions for Pseudo-Potential Basis Sets of the Transition Metals Sc–Cu, Y–Ag and La–Au. *Chem. Phys. Lett.* **1993**, 208, 111–114.
- (55) Hehre, W. J.; Ditchfield, R.; Pople, J. A. Self—Consistent Molecular Orbital Methods. XII. Further Extensions of Gaussian—Type Basis Sets for use in Molecular Orbital Studies of Organic Molecules. *J. Chem. Phys.* **1972**, *56*, 2257–2261.
- (56) Gorelsky, S. AOMix Program for Molecular Orbital Analysis, version 6.5; University of Ottawa: Ottawa, Canada, 2011.
- (57) Gorelsky, S. I.; Lever, A. Electronic Structure and Spectra of Ruthenium Diimine Complexes by Density Functional Theory and INDO/S. Comparison of the Two Methods. *J. Organomet. Chem.* **2001**, *635*, 187–196.
- (58) Krishnan, R.; Binkley, J. S.; Seeger, R.; Pople, J. A. Self-Consistent Molecular Orbital Methods. XX. A basis Set for Correlated Wave Functions. *J. Chem. Phys.* **1980**, 72, 650–654.